$\mu^+ \to e^+\gamma$ Experiment
Technical Note No.15

Technical Report on the COBRA Magnet

Wataru Ootani [a], Yasuhiro Makida [b], Satoshi Mihara [a],
Toshiya Mitsuhashi [a], Roger Ruber [b1], and Akira Yamamoto [b]

[a] *International Center for Elementary Particle Physics, University of Tokyo, 7-3-1 Hongo, Bunkyo-ku, Tokyo 113-0033, Japan*

[b] *High Energy Accelerator Research Organization (KEK), 1-1 Oho, Tsukuba, Ibaraki 305-0801, Japan*

Abstract

The design of the magnet for the positron spectrometer for the $\mu \to e\gamma$ experiment (COBRA magnet) is described in this note. One of the most important issues on the magnet design is the suppression of the stray magnetic field in the vicinity of the liquid xenon photon detector. Small stray field is quite essential for the proper operation of the photon detector. The stray magnetic field can be sufficiently suppressed by using compensation coils while keeping the good features of the positoron spectrometer described in the proposal[1]. The results from the detailed mechanical analysis on the magnet and experimental tests on the mechanical property of the magnet are described.

[1]Present address: University of Uppsala, 535, Thunbergsvgen 5, S-751 21 Uppsala, Sweden

1 Overview of the design of the COBRA magnet

The schematic view of the COBRA magnet are shown in Fig. 1 where other detector components are also shown. Fig. 2 shows the layout of the coils in the magnet with the dimensions. The COBRA magnet consists of the main superconducting magnet and a pair of compensation coils which is adopted to reduce the stray magnetic field around the photon detector. The superconducting magnet consists of the five coils with three different radii; one central coil, two gradient coils, and two end coils. A resistive coil will be used for the compensation coil.

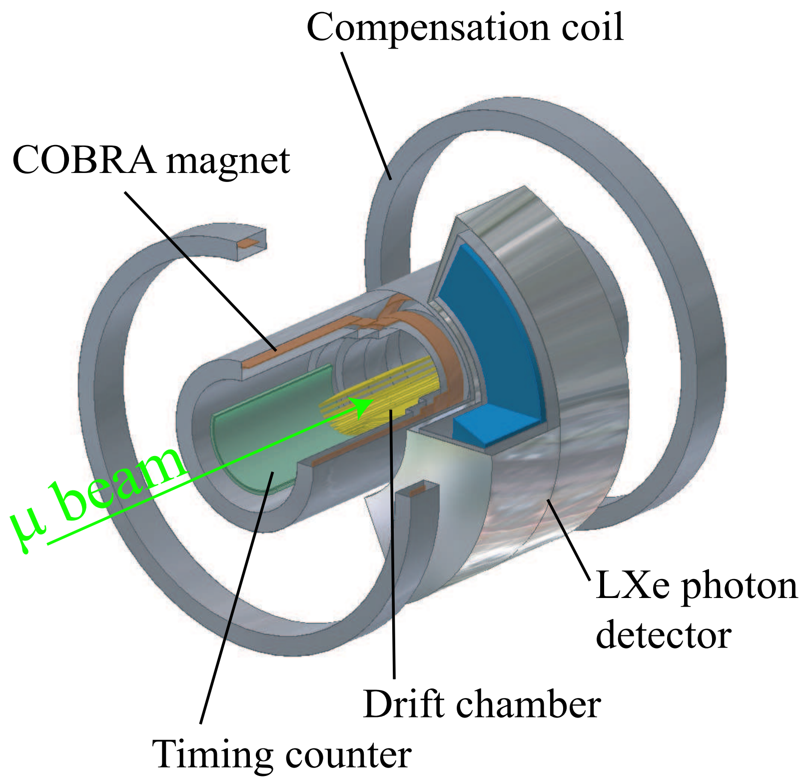

Figure 1: Schematic view of the $\mu \to e\gamma$ detector with compensation magnet

The magnet is specially designed to form a gradient magnetic field to realize the good features of the positron spectrometer such as the constant bending radius of the positrons and quick sweep of the positrons. A step structure in the central region of the main magnet is adopted instead of the sand-glass structure as described in the proposal[1] because the magnet with such structure is technically easier to construct.

The parameters of the COBRA magnet are listed in Table 1. Fig. 3 shows the contour plot of the magnetic field distribution produced by the COBRA magnet. The profile of the distribution along the magnet axis is shown in Fig. 4. The performance of the spectrometer and stray field around the photon detector were optimized by adjusting the diameter, length, and current density of the coils. The five superconducting coils are connected in series and the current density of the coil is controlled by changing the density of the cable winding and operating current as summarized in Table 1 The current density in the inner part of the end coil with a length of 20 cm is smaller than that in the outer part of the end coil. It also serves to reduce the stray field in the region of the photon detector efficiently. The performance of the spectrometer based on this design of the COBRA magnet and the stray field around the photon detector will be described in Sec. 3 and Sec. 4, respectively.

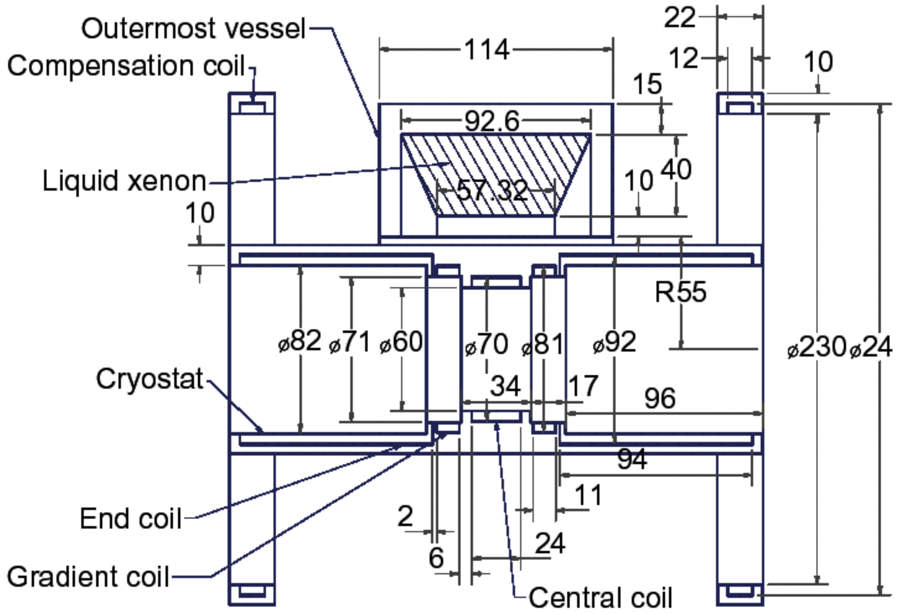

Figure 2: Layout of the COBRA magnet with the compensation coils.

Table 1: Parameters of the COBRA magnet.

Coil	Central	Gradient	Inner end	Outer end	Compensation
Conductivity	Super	Super	Super	Super	Resistive
Inner dia. (mm)	700	810	920	920	2210
Outer dia. (mm)	712.4	820.6	929.5	929.5	2590
Length (mm)	240.3	110.4	189.9	749.2	265
Layers	4	4	3	3	14
Turns per layer	267	123 (1st) 92(2nd-4th)	80	624 (1st-2nd) 92(3rd)	20
Turns (total)	1068	399	240	1548	280
Winding [2]	e-w	e-w(1st) f-w(2nd-4th)	f-w	f-w	double pancake
Inductance(H)	1.64	0.62	0.35	2.29	0.54
$I_{\rm op}$(A)	360	360	360	360	360
Energy E (kJ)	106	40	23	148	35
Weight M (kg)	9	4	7	28	1620
E/M (kJ/kg)	11.8	10.0	3.3	5.3	0.02

[2] e-w : edge-wise f-w : flat-wise

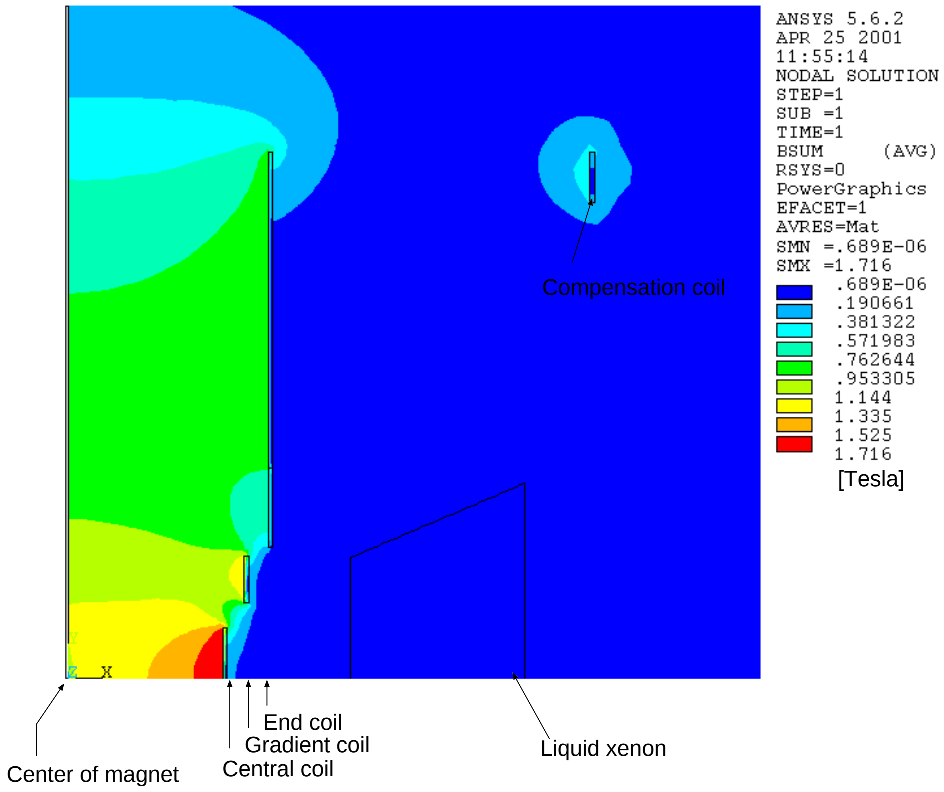

Figure 3: Contour plot of the magnetic field produced by the COBRA magnet.

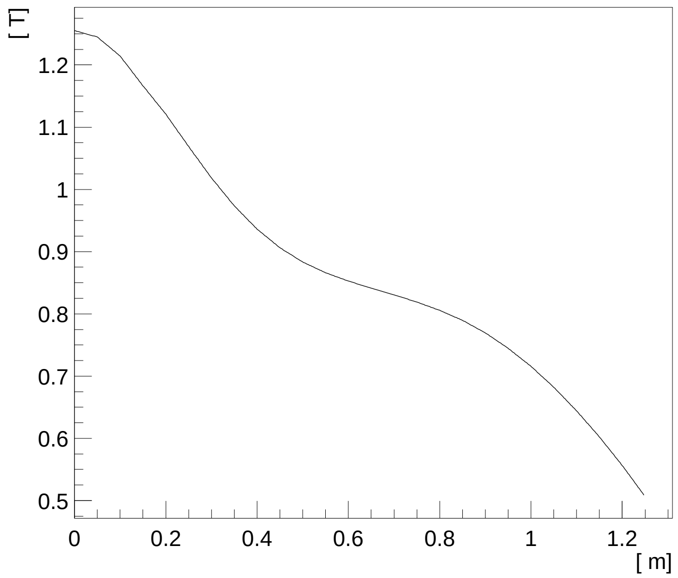

Figure 4: Profile of the magnetic field along the magnet axis.

2 Development of the superconducting cable

A high-strength aluminum-stabilized superconducting cable was developed for the COBRA magnet. Fig. 5 shows the cross-sectional view of the cable. The cable consists of NbTi multi-filament embedded in copper matrix and aluminum-stabilizer. The aluminum-stabilizer is mechanically reinforced by "micro-alloying" technology. The aluminum-stabilizer can be reinforced by adding small amount of metals such as nickel, magnesium, and copper while keeping electrical resistivity as low as possible[2]. Nickel of 5000 ppm is added into the aluminum-stabilizer in the superconducting cable for the COBRA magnet.

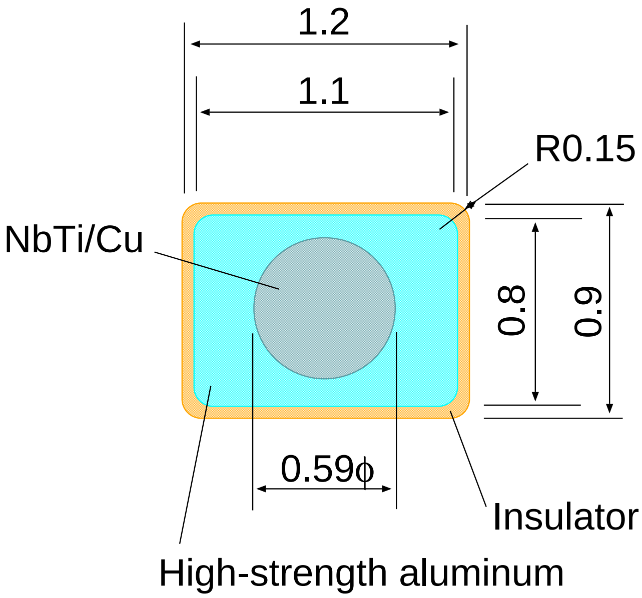

Figure 5: Cross-sectional view of the high-strength aluminum-stabilized superconducting cable developed for the COBRA magnet.

The performance of the superconducting cable was measured around 4 K. The parameters of the superconductor are summarized in Table 2. An overall yield strength of the cable was found to be above 220 MPa at 4.2 K while keeping the Residual Resistivity Ratio (RRR) [3] above 280. The characteristics of superconductivity were also measured. Fig. 6 shows the measured critical current as a function of the applied magnetic field. The operating current will be 360 A and the peak value of the magnetic field is 1.7 T in the central coil. The load line of the COBRA magnet with the operating point is also shown in Fig. 6. Since the operating temperature of the coil is estimated to be about 5 K, this figure indicates that the performance of the cable has a safety margin of about 30% compared to the operating condition of the COBRA magnet.

[3]Ratio of the bulk resistivity at room temperature to the normal conducting resistivity at 4K

Table 2: Parameters of the superconducting cable developed for the COBRA magnet.

Conductor material	NbTi/Cu
NbTi/Cu diameter	0.59 mm
NbTi/Cu Cu ratio	0.82
Insulator	Kapton polyimide tape
Overall cross section	$0.8 \times 1.1\,\mathrm{mm}^2$
Overall cross section with insulator	$0.9 \times 1.2\,\mathrm{mm}^2$
Critical current density	$5476\,\mathrm{A/mm}^2$ at 4.2 K, 2.0 T
Critical current	851 A at 4.2 K, 2.0 T 666 A at 5.0 K, 2.0 T
RRR	Cu 55.9 Al 280
0.2 % yield strength (conductor)	598 MPa at 4.2 K
0.2 % yield strength (Al stabilizer)	105 MPa at 4.2 K
0.2 % yield strength (overall)	221 MPa at 4.2 K

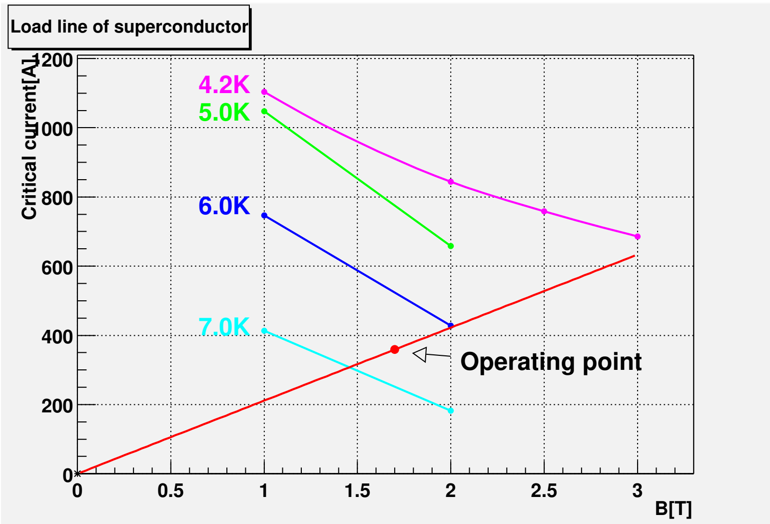

Figure 6: Measured critical current as a function of the applied magnetic field. The load line and operating point for the COBRA magnet are also shown.

3 Suppression of the stray field

The stray field from the superconducting magnet could degrade the performance of the liquid xenon photon detector because the PMT gain rapidly drops as the strength of the applied magnetic field increases. Fig. 7 shows the relative output of the PMT to be used in the liquid xenon photon detector (HAMAMATSU R6041Q) as a function of the magnetic field[3] where the z-axis is defined as the PMT axis. The tolerance to the magnetic field of the PMT strongly depends on the direction of the applied magnetic field compared to the tube axis. There is strong dependence even on the direction on the photo-cathode plane due to the structure of the dynodes. The maximum allowed strengh of the magnetic field is 150 Gauss and 50 Gauss respectively for the perpedicular and parallel directions to the tube axis. The maximum allowed strength is defined as the field strength where the relative gain of the PMT is reduced by 50 %.

Therefore, the stray field should be reduced down to 50 Gauss level in the vicinity of the photon detector.

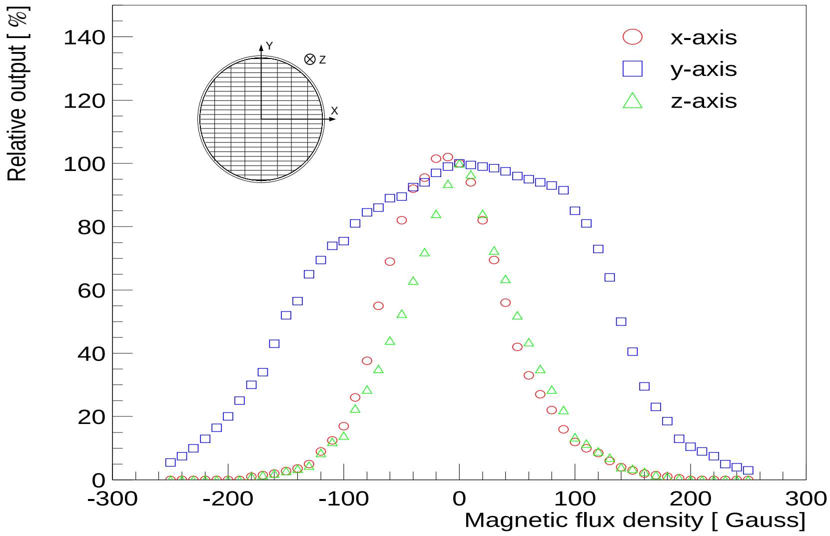

Figure 7: Relative output of the PMT to be used in the photon detector as a function of the applied magnetic field. [3]. The z-axis is defined as the PMT axis here.

At the early stage of the design work on the COBRA magnet we had investigated the shielding of the stray field by using an iron return yoke. It was not, however, possible to suppress the stray field bellow the acceptable level mainly due to the local leakage field coming from the step structure of the magnet. Other demerit of the return yoke is that very massive iron is necessary and electromagnetic interactions among the COBRA magnet, beam transport magnet, and yoke have to be carefully managed.

We currently adopt the active shielding of the stray field by using a pair of compensation coils as described in Sec.1. The direction of the operating current for the compensation coil is same as that for the main magnet. The magnetic field around the photon detector can be canceled effectively by the compensation coil because the shape of the flux lines produced by the compensation coil is very similar to that produced by the main magnet in the region of the photon detector. Fig.8 shows the contour plot of the magnetic field produced by the COBRA magnet with the compensation coils. It can be seen the residual field is very small all over the photon detector region.

Fig.9 shows the profile of the magnetic field at the PMT position. The horizontal axis shows the length from the point of $z = 0\,\mathrm{cm} and r = 62\,\mathrm{cm}$ along the boundary path right outside the PMT array wall on the horizontal plane including the magnet axis. It is measured up to the point of $z = 0\,\mathrm{cm} and r = 108\,\mathrm{cm}$. The component of the magnetic field parallel and perpendicular to the PMT axis are separately shown. Note that the PMTs on the side wall of the calorimeter are arranged so that the axis is parallel to the magnet axis. The maximum allowed strength for each component is also shown by dashed lines. It can be seen that the field strength at the PMT position is well below the acceptable level.

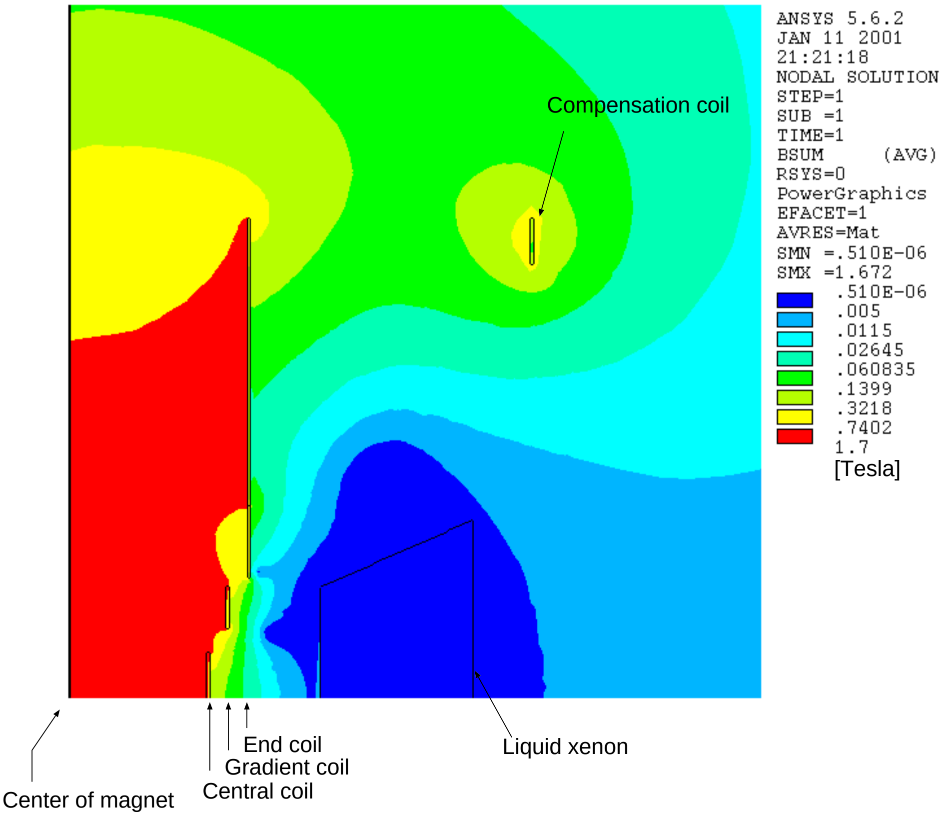

Figure 8: Contour plot of the residual magnetic field. A box in the photon detector region shows the boundary where the PMTs are arranged. Note that the contour interval is not linear.

4 Performance of the spectrometer with the current design of the COBRA magnet

In this section we discuss the positron tracking in the magnetic field distribution produced by the current design of the COBRA magnet with the compensation magnet. The simulation is performed by using GEANT[4]. The projected bending diameter of the signal positron of 52.8 MeV should be constant independently of the emission zenith angle. Fig.10 shows the distribution of the bending diameter for the signal positrons with the emitting zenith angle of $0.08 \leq \cos\theta \leq 0.35$. The bending diameter is measured by the maximum value of the radial distance from the magnet axis. The spread of the muon beam of $\sigma_x = \sigma_y = 0$ mm($\sigma_x = \sigma_y =$ 5 mm) is assumed for the distribution with(without) hatch. The fluctuation of the bending diameter caused by the magnetic field gradient is estimated to be 1.2 mm(rms) which is much smaller than the fluctuation caused by the muon beam spread.

The hit rate of the Michel positorons at the drift chamber was calculated under the current design of the COBRA magnet. Fig. 11 shows the hit rate as a function of radius assuming a muon decay rate of $1 \times 10^8 \mathrm{sec}^{-1}$. The drift chamber will be placed from 19.5 cm to 28 cm. Stable chamber operation is possible under this level of hit rate.

Fig.12 shows the distribution of z of the impact point on the timing counter as a function of $\cos\theta$ where the counter is placed at $22.5 \leq |z| \leq 120$ cm and $r = 29.5$ cm. The muon beam spread is not taken into account. The incident point on the timing counter ranges at $23 \leq |z| \leq 95$ cm.

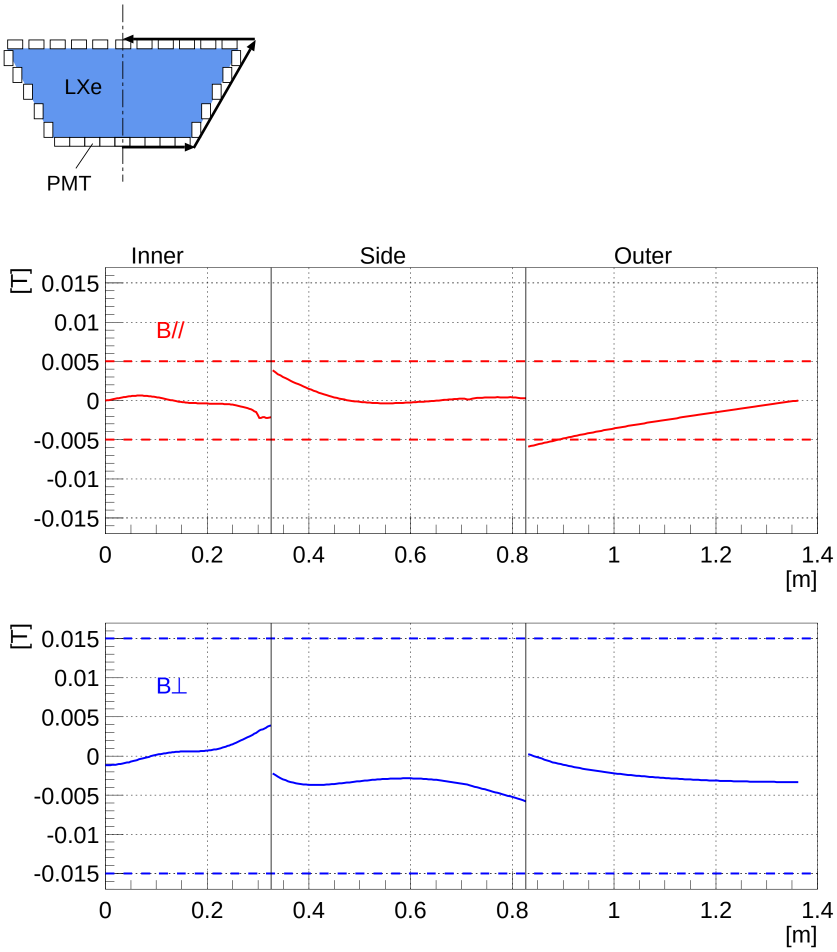

Figure 9: Profile of the magnetic field along the boundary path of the liquid xenon photon detector where the PMTs are arranged. The top(bottom) figure is the profile of the component parallel(perpendicular) to the tube axis. The maximum allowed levels are also drawn with dashed lines.

Fig.13 shows the azimuthal angle of the impact point on the timing counter as a function of $\cos\theta$ where emitting azimuthal angle of $-60^\circ \leq \phi \leq 60^\circ$ and the spread of the muon beam of $\sigma_x = \sigma_y = 5\,\mathrm{mm}$ are assumed. The azimuthal angle of -90° corresponds to the downward vertical direction. It shows the occupancy on the azimuthal angle of the timing counter should be $-130^\circ \leq \phi \leq 15^\circ$.

The hit rate of the timing counter due to the Michel positrons is estimated with the counter placed at $27.5\,\mathrm{cm} \leq |z| \leq 125\,\mathrm{cm}$ and $r = 29.5\,\mathrm{cm}$. The simulation shows $6.5\,\%$ of the Michel positrons are incident to the scintillator at forward and backward sides. The hit rate is higher by $60\,\%$ compared with that in the magnet geometry in the proposal. However, since the incident point of the signal positron on the scintillator extends up to $z = 100\,\mathrm{cm}$ for the positrons with $\cos\theta \leq 0.35$ in the present magnet design with the muon beam spread, the accidental hit rate can be reduced down to $4\,\%$ by using the shorter scintillator.

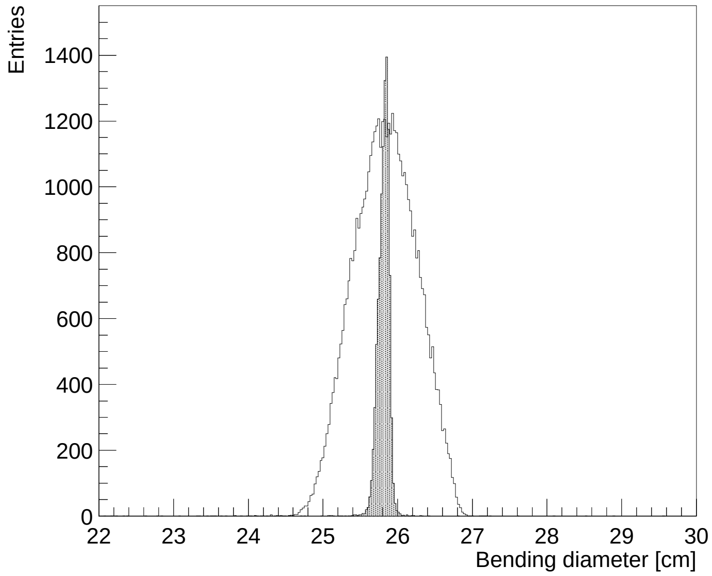

Figure 10: Distribution of the bending diameter of the signal positrons. The distribution with(without) hatch is obtained with the muon beam spread of $\sigma_x = \sigma_y = 0\,\mathrm{mm}$ ($\sigma_x = \sigma_y = 5\,\mathrm{mm}$).

5 Mechanical design of the COBRA magnet

Fig. 14 shows the coils, support shell of the coils, and cryostat. This design was optimized by the detailed mechanical calculations and related experimental tests which will be described here.

Table 3 shows the calculated electromagnetic force acting on each coil. The stress due to the electromagnetic force is maximized around both edges of the support shell of the central coil. In order to reduce the stress around that region, a thin support cylinder bypassing over the central coil (bypassing support) is adopted as shown in Fig. 14. The shape and thickness of the support shell and bypassing support were optimized to make the mechanical stress acceptable for the materials used in the magnet. Fig.15 shows the calculated stress distribution around the central coil and bypassing support. The result indicates the maximum stress is 74 MPa at the edge of the support shell for the central coil which is well below the maximum allowed stress, 100 MPa at 4K for the aluminum (A5083P) to be used for the support shell.

Table 3: Electromagnetic force acting on the coil.

	Axial force (ton)	Hoop stress (MPa)
Central coil	13.1	66
Gradient coil	4.2	53
End coil	15.3	46

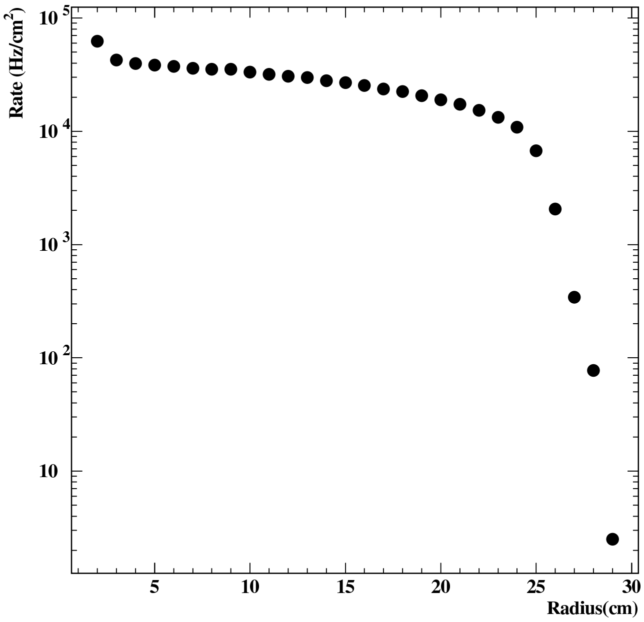

Figure 11: Hit rate of the Michel positrons at the drift chamber under the magnetic field distribution produced by the COBRA magnet.

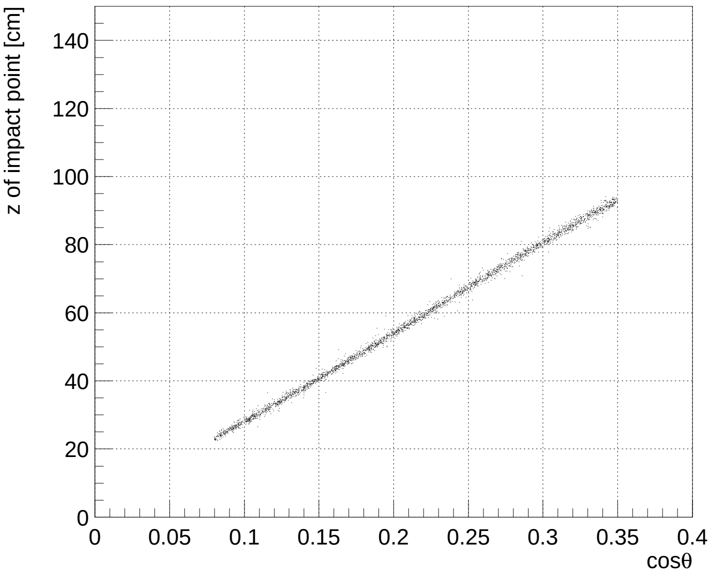

Figure 12: Distribution of z of the impact point on the timing counter as a function of $\cos\theta$.

Various mechanical tests for some essential parts in the magnet are being performed to verify the validity of the current design of the magnet.

In order to test the strength of glueing between the coil and aluminum support structure against the axial component of the electromagnetic force, shearing tests were performed using

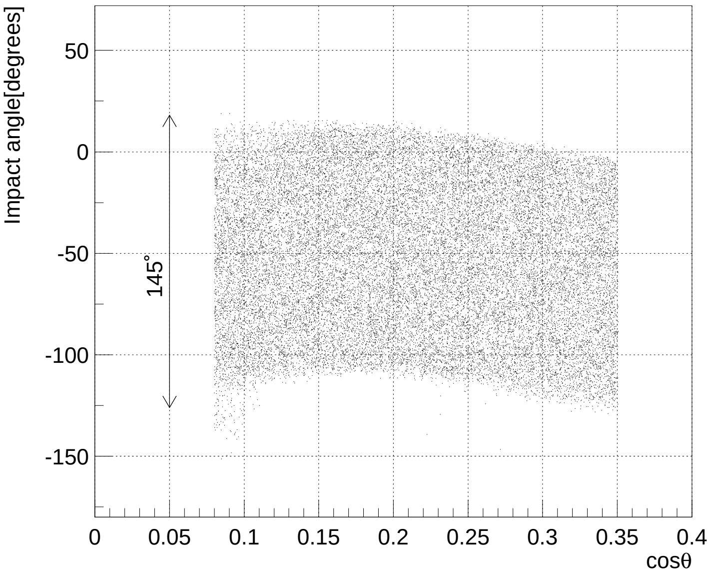

Figure 13: Distribution of ϕ of the impact point on the timing counter as a function of $\cos\theta$ where the emitting angle of $-60° \leq \phi \leq 60°$ and the spread of the muon beam of $\sigma_x = \sigma_y =$ 5 mm are assumed.

a small model coil glued to the aluminum support cylinder with an epoxy resin. The setup for the test is illustrated in Fig. 16. The diameter and length of the model coil are 50 mmϕ and 42 mm(34 turns), respectively. Shearing force was loaded to the coil along the coil axis with the support ring fixed. The strength of the force was increased until the glueing between the coil and support cylinder was ruptured. Six samples with different thickness of the epoxy resin between the coil and support cylinder were tested at liquid nitrogen temperature. The average of the breaking stress is 7.8 MPa. The level of the breaking stress is almost acceptable and could be improved by using another type of insulating tape.

The mechanical strength of the bypassing support which will carry the greater part of the axial force acting on the end coil and gradient coil (17.4 ton) was also measured. A test cylinder with the same geometry as the bypassing support was used in this test. That is made of aluminum and has the diameter of 852 mm and length of 390 mm. The axial force loaded on the test cylinder was increased until the cylinder buckled (Fig. 17). The measured buckling stress was 68 MPa which is well below the predicted value of 44MPa by stress calculations.

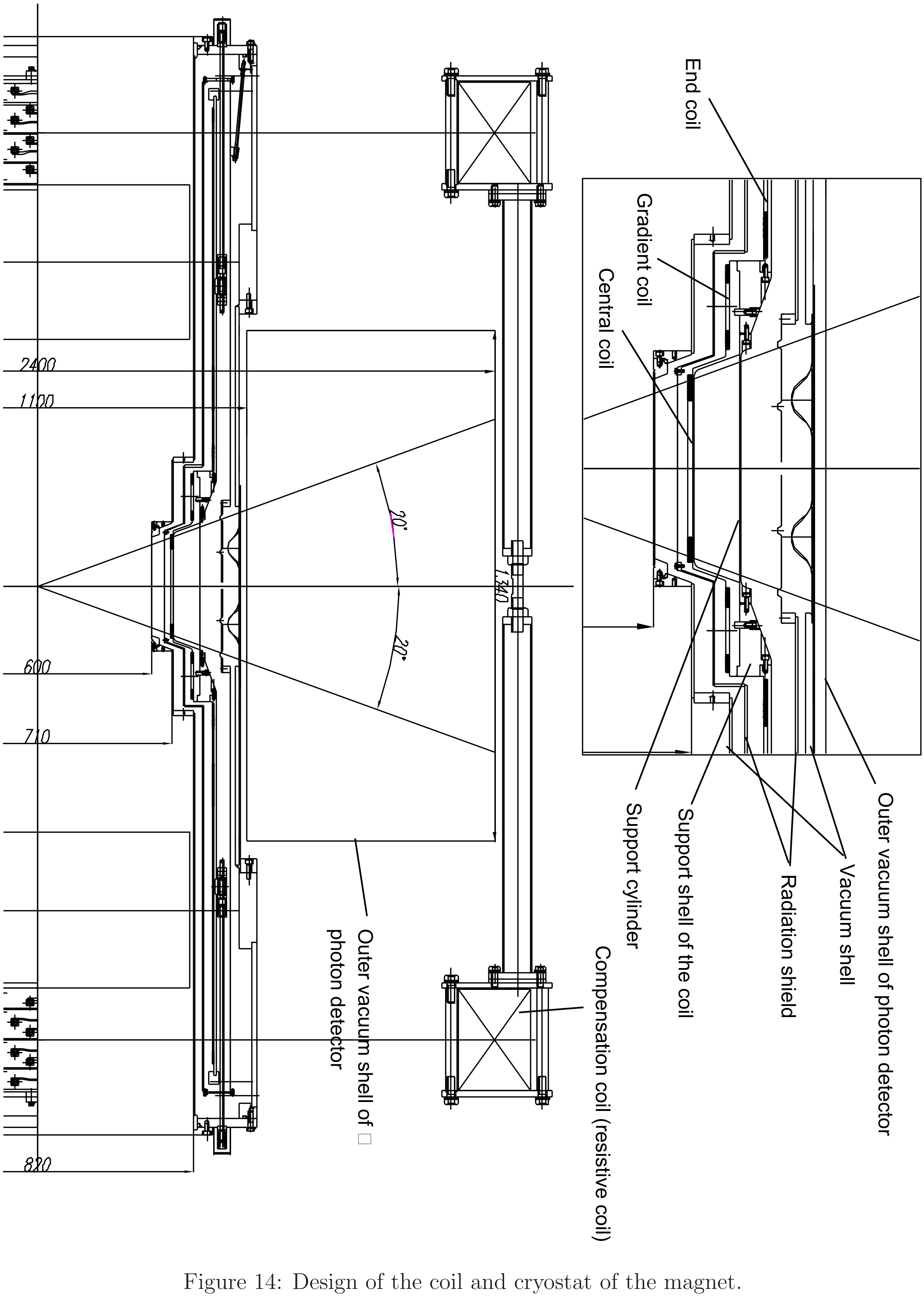

Figure 14: Design of the coil and cryostat of the magnet.

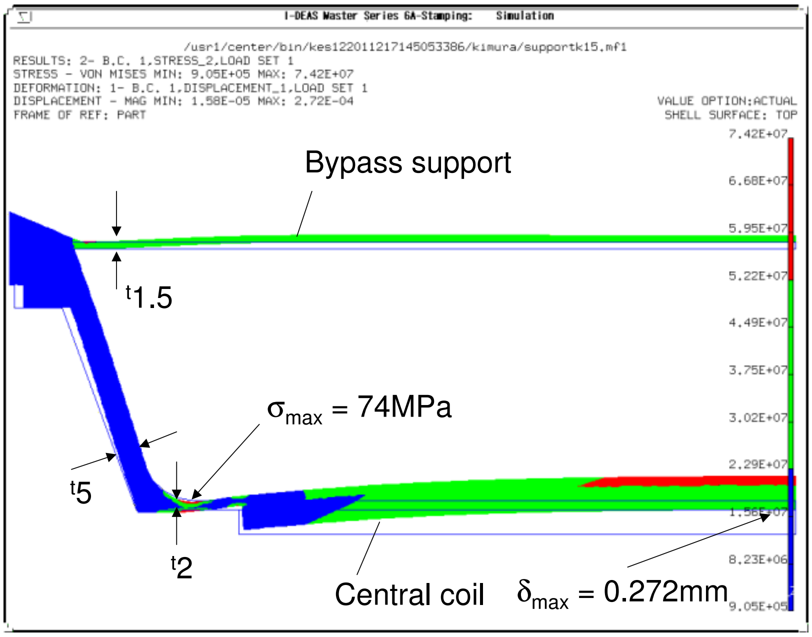

Figure 15: Stress distribution around the central coil of the magnet.

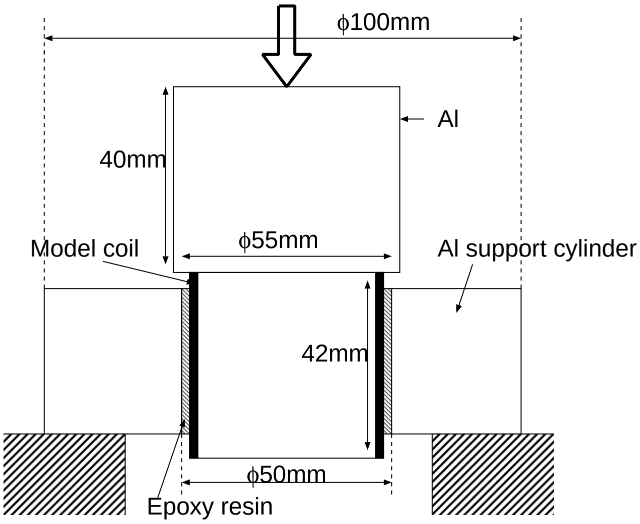

Figure 16: Setup for the shearing test of the glueing between the coil and support structure.

6 Transparency of the magnet

Thanks to the the high-strength superconductor developed for the COBRA magnet, we can minimize the thickness of the support structure required for a given electromagnetic force acting on the coils. The components used in the coil and cryostat of the magnet within the acceptance of the photon detector are listed with their thickness in Table 4. The thickness of the magnet is increased by 42 % compared to that in the proposal. The increase is mainly due to the additional supporting cylinder (bypassing support) as described in Sec. 5 and change in the winding way. Since the coil radius is shrunk by around 10 % compared to that in the proposal, the central magnetic field has to be increased by about 10 %. In order to minimize the

Figure 17: Support cylinder after the buckling occurred.

increase of the operating current for increasing the central field strength, the superconducting cable was wound in the "edge-wise" way in the central coil instead of the usual "flat-wise" way. These two kinds of ways to wind the cable are illustrated in Fig.18. We can obtain the stronger central field by the edge-wise winding with the same operating current. However, if this winding way is adopted, we have to accept the increase of the material thickness of the central coil by $2.6 \times 10^{-2} X_0$.

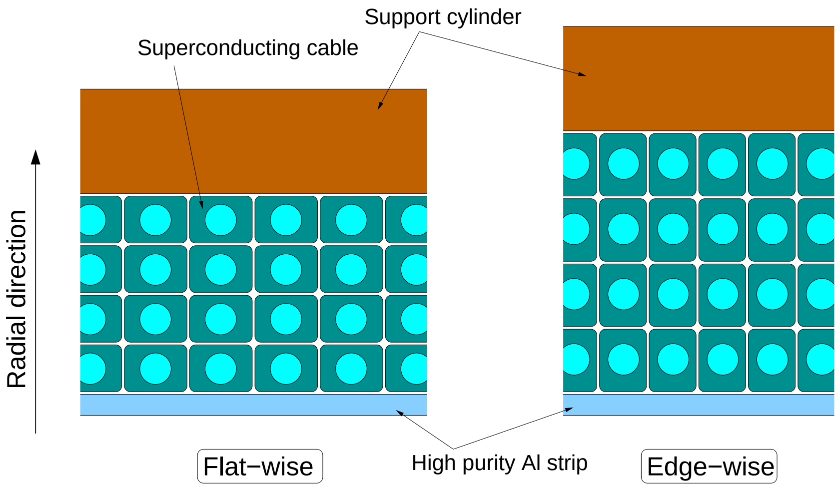

Figure 18: Flat-wise and edge-wise winding.

Table 4: Transparency of the COBRA magnet.

	Equivalent thickness g/cm^2	Radiation thickness X_0
Coil		
Conductor(Al)	0.745	0.0312
Conductor(NbTi/Cu)	0.868	0.0766
Insulation(Uplex/G-Epp)	0.069	0.0020
Epoxy-resin	0.058	0.001
Support cylinder	0.945	0.0396
Pure Al strip	0.068	0.003
Subtotal	2.753	0.153
Cryostat		
Outer vacuum shell	0.405	0.017
Radiation shield	0.162	0.007
Inner vacuum shell	0.405	0.017
Super insulation	0.105	0.003
Subtotal	1.192	0.048
Total	3.83	0.197

7 Summary

The current design of the magnet for the positron spectrometer for the $\mu \rightarrow e\gamma$ experiment (COBRA magnet) was described. In this design the stray magnetic field is successfully suppressed in the vicinity of the liquid xenon photon detector by using compensation coils. It is quite essential for the proper operation of the photon detector. The performance of the spectrometer based on the current design of the COBRA magnet was also evaluated and no major problem was found. Detailed mechanical analysis was done to optimize the design of the coil support structure and cryostat of the magnet. Some experimental tests were performed and the results indicate there is no problem in the current mechanical design of the magnet.

References

[1] "Search for $\mu^+ \rightarrow e^+\gamma$ down to 10^{-14} branching ratio", Research Proposal to Paul Scherrer Institut, May 1999 (PSI Proposal R-99-05.1).

[2] A. Yamamoto et al., Nucl. Phys. **B78** (1999) 565–570.

[3] The tolerance to the magnetic field was measured by the Hamamatsu Photonics.

[4] GEANT, Detector Description and Simulation Tool, CERN Program Library.